

# A numerical study of Haar wavelet priors in an elliptical Bayesian inverse problem

Wacker, Philipp\*      Knabner, Peter†

May 18, 2022

## Abstract

Wavelet (Besov) priors are a promising way of reconstructing indirectly measured fields in a regularized manner. We demonstrate how wavelets can be used as a localized basis for reconstructing permeability fields with sharp interfaces from noisy pointwise pressure field measurements. For this we derive the adjoint method of minimizing the Besov-norm-regularized misfit functional (this corresponds to determining the maximum a posteriori point in the Bayesian point of view) in the Haar wavelet setting.

## 1 Introduction

We imagine we want to infer some unknown (typically infinite-dimensional) quantity  $u$  by their effect (through some “forward map”) on a noisy observed quantity  $y$  (in general finite-dimensional), i.e.

$$y = G(u) + \eta \tag{1}$$

where  $\eta$  is observational noise. By dimensionality and randomness, this is a vastly ill-posed problem in dire need of some sort of regularization. For a classical regularization approach, see [21], or in the context of groundwater inference, [48]. In the Bayesian context, this means choosing a prior model describing our belief concerning a-priori feasible values of  $u$ . Then, Bayes’ theorem allows us to incorporate the observation  $y$  in order to obtain the posterior distribution  $u|y$ . In many applications, the inverse problem consists of inferring a function (i.e. a permeability or density scalar field over some domain) by their effect on some observation through a PDE-governed dynamics. This raises the question, “what are random functions?”

This is a very subtle question and even its simplification, “what are Gaussian random functions?”, is very difficult to answer (see [6] and [33]) and full of pitfalls due to the infinite dimensionality of function spaces.

In the Gaussian setting, there are basically two ways of defining random functions: Either by interpreting them as samples from a Gaussian random field which can be uniquely defined by its mean field and covariance function, or by defining an abstract Gaussian measure on a vector space of functions, uniquely determined by a mean function and a covariance operator. The latter view intuitively corresponds to defining a random function as a randomized superposition of deterministic

---

\*Friedrich-Alexander-Universität Erlangen-Nürnberg, [phkwacker@gmail.com](mailto:phkwacker@gmail.com)

†Friedrich-Alexander-Universität Erlangen-Nürnberg

basis functions of the function space (e.g. a trigonometric basis, this corresponds to the Gaussian prior in section 2.3). This is due to the fact that any Gaussian measure on a Banach space has a white noise expansion (see [11, Theorem 2.12]).

A relatively new (non-Gaussian) function space prior is the Besov prior (which we will call Wavelet prior in this paper, for reasons stated below) described mathematically in [12], [34] and practically demonstrated in one dimension in [7]. The main idea of this prior is that a random function sampled from this prior is given by a random superposition of localized basis functions (a set of compactly supported wavelets) in contrast to the non-local trigonometric basis functions often employed.

This article is supposed to build the bridge to higher dimensions, in particular  $d = 2$ , and show that Wavelet priors are able to reconstruct essential information about permeability fields with sharp interfaces in the inverse elliptical problem setting in reasonable computing time. This is the main benefit of this approach: Reconstructions using Gaussian priors based on trigonometric expansions will invariably lead to smoothed reconstructions of jumps. In this study, we will restrict ourselves to the Haar wavelet basis so that we can use its discontinuity to model interfaces. Wavelets have been employed in a groundwater inference setting in [10], but their approach differs in philosophy from the Bayesian wavelet prior notion in that they employ a template matching algorithm using training images. There is also recent progress in the field of medical imaging using Besov priors [42]. An introduction into sampling from Besov priors is [50]. The use of wavelets in inverse problems is not entirely new, see [43], but here wavelets were used in the context of multilevel methods.

## 2 The inverse elliptical problem

### 2.1 General Bayesian inverse problems

The inverse problem we are interested in is defined as follows<sup>1</sup>. The goal is to recover the unknown parameters  $u \in X$  from a noisy observation  $y \in Y$  where

$$y = G(u) + \eta \tag{2}$$

with the so-called forward response map  $G : X \rightarrow Y$  which often – and in our case – is a PDE solution operator. We denote by  $X$  and  $Y$  separable Hilbert spaces and by the random variable  $\eta$  the observational noise.

Inverse Problems arise in a multitude of applications, for example in geosciences, medical imaging, reservoir modelling, astronomy and signal processing. A probabilistic approach has been undertaken first by Franklin [24], Mandelbaum [37] and others, and a formulation of inverse problems in the context of Bayesian probability theory was originally obtained by Fitzpatrick [23]. More recent literature about inverse problems in the Bayesian setting can be found in [39], [45], [29]. See also [9] for probabilistic groundwater estimation from a more applied viewpoint.

In the following, due to the nature of the inverse problem we are interested in, we assume that the number of observations is finite, i.e.  $Y = \mathbb{R}^K$  for some  $K \in \mathbb{N}$ , whereas the unknown is a distributed quantity, which is a typical setting for many applications mentioned above. Thus, the inverse problem consists of inferring infinitely many parameters from a finite number of noisy observations. This leads to an ill-posed problem (this is also often true for the case of infinitely many

---

<sup>1</sup>we follow the exposition of the inverse problem in [5]

observations, as in the case of the inverse heat equation, see [45]), which needs to be regularized. We will focus here on the Bayesian approach, i.e. the inverse problem becomes well-posed by a prior distribution on the feasible values for  $u$  and the data gets incorporated by a Bayesian update on this prior measure, yielding the posterior measure in result. Furthermore, we assume that the observational noise is Gaussian, i.e.  $\eta \sim N(0, \Gamma)$  with a symmetric, positive definite matrix  $\Gamma \in \mathbb{R}^{K \times K}$ .

We consider the least squares “error” (or model-data misfit) functional

$$\Phi(u; y) = \frac{1}{2} \|\Gamma^{-1/2}(y - G(u))\|_Y^2, \quad (3)$$

where  $\Gamma$  normalizes the model-data misfit and is normally chosen as the covariance operator of the noise. Plain infimization of this cost functional is not feasible due to the ill-posedness of the problem. For a given prior  $u \sim \mu_0$ , we derive the posterior measure  $u|y \sim \mu$  where

$$\mu(du) = \frac{1}{Z} \exp(-\Phi(u; y)) \mu_0(du). \quad (4)$$

For a derivation of this fact, see either [25] or, in the specific case of the linear inverse elliptical problem, [13]. An issue of Bayesian inverse problems is how to obtain useful information from the posterior, which is in general given by (4), i.e. abstractly as a density w.r.t. the prior. Most quantities of interest can be computed by sampling, for example with Metropolis-Hastings methods.

The *maximum-a-posteriori point* plays a key role as a “point of maximum density” (although this does not make rigorous sense in the infinite dimensional setting). In the case where the prior measure is Gaussian with Cameron-Martin space  $(E, \|\cdot\|_E)$  it is defined by

$$u_{\text{MAP}} := \operatorname{arginf} I(u)$$

where  $I(u) = \Phi(u) + \frac{1}{2} \|u\|_E^2$ . In the non-Gaussian setting, there are generalizations [29]. Our simulations will mostly show the computed value of  $u_{\text{MAP}}$ . Another interesting quantity is the *conditional mean*, which is

$$u_{\text{CM}} := \mathbb{E}^\mu u.$$

In general,  $u_{\text{CM}}$  and  $u_{\text{MAP}}$  can be vastly different. Typically, the MAP point can exhibit sparse behaviour (if the corresponding optimization problem warrants this), but the Conditional Mean (as well as samples of the posterior) will often fail to have this property. This serves as a general caveat to “sparse Besov priors”.<sup>2</sup>

## 2.2 The model inverse elliptical problem

Our model inverse problem will be the following: Given a solution  $p$  of

$$\begin{aligned} -\nabla \cdot (e^{u(x,y)} \cdot \nabla p(x,y)) &= f(x,y) \text{ in } [0,1]^2 \\ p(x,y) &= g(x,y) \text{ on } \Gamma_D \\ \partial_\nu p(x,y) &= h(x,y) \text{ on } \Gamma_N \end{aligned}$$

( $\Gamma_D \cup \Gamma_N = \partial[0,1]^2$  is the decomposition of the boundary in Dirichlet and Neumann boundary) to some permeability field  $\theta = e^u \in L^\infty([0,1]^2)$  (the field  $u$  is called the logpermeability), we assume

---

<sup>2</sup>thanks to Youssef Marzouk who pointed this out to me.

that we have noisy pointwise observations  $y_i = p(x_i, y_i) + \eta_i$ ,  $i = 1, \dots, N$  with  $\eta_i \sim N(0, \gamma^2)$  i.i.d. The inverse problem is the inference

$$\mathbb{R}^N \ni (y_i)_{i=1}^N \mapsto u \in L^\infty([0, 1]^2),$$

i.e. we want to find the unknown logpermeability field  $u$  from pointwise observations of the corresponding pressure field. The inference of an infinite-dimensional quantity from finite-dimensional one is obviously ill-posed, hence the need for a regularization, in our case a prior.

In the language of the last section,  $\Phi(u; y) = \frac{1}{2\gamma^2} \|y - \Pi p\|^2$  where

$$\Pi p = (p(x_1, y_1), \dots, p(x_N, y_N))^T$$

is the evaluation operator and  $y = (y_i)_{i=1}^N$  is the observation vector. The survey paper by Delhomme et al [17] and Sun's book about inverse problems [47] give a thorough introduction into the evolution of inverse problems in the geohydrology community.

### 2.3 A common prior: $N(\mu, \beta(-\Delta)^{-\alpha})$ . Motivation for Wavelet priors

A well-studied prior is the Gaussian  $N(\mu, \beta(-\Delta)^{-\alpha})$  prior for  $\alpha > d - \frac{1}{2}$  and  $\beta > 0$  (see, for example, [14]). This corresponds to a prior whose samples are randomized weighted Fourier expansions: We say that  $v \sim N(\mu, \beta(-\Delta)^{-\alpha})$  in one dimension, if

$$v(x) = \mu + \beta \cdot \sum_{k \in \mathbb{N}} [\varepsilon_k \cdot k^{-\alpha} \sin(2\pi kx) + \zeta_k \cdot k^{-\alpha} \cos(2\pi kx)],$$

where  $\varepsilon_k, \zeta_k \sim N(0, 1)$  i.i.d. This is immediate from the Karhunen-Loève expansion of the Gaussian measure. The two-dimensional analogue is

$$\begin{aligned} v(x, y) = \mu + \beta \cdot \sum_{k \in \mathbb{N}} [\varepsilon_k \cdot k^{-\alpha} \sin(2\pi kx) \sin(2\pi ly) + \zeta_k \cdot k^{-\alpha} \cos(2\pi kx) \sin(2\pi ly) \\ + \eta_k \cdot k^{-\alpha} \sin(2\pi kx) \cos(2\pi ly) + \theta_k \cdot k^{-\alpha} \cos(2\pi kx) \cos(2\pi ly)] \end{aligned}$$

with  $\varepsilon_k, \zeta_k, \eta_k, \theta_k \sim N(0, 1)$  i.i.d. As the trigonometric functions build an orthonormal basis for  $L^2([0, 1]^d)$ , this prior is in principle able to reproduce any permeability function, but the fact that the covariance operator is diagonal over the Fourier basis leads to a certain type of samples which may be unsuitable in some applications:

Subsurface topology is dominated by “sheets” of fairly homogenous permeability with sharp (discontinuous) interfaces inbetween (think of a granite layer next to a clay layer). Inference of such a geometry by a Gaussian prior with a Laplacian covariance operator suffers the usual drawbacks of Fourier analysis when applied to “jumpy” signals: Sharp interfaces are either not well represented or the Gibbs phenomenon leads to unphysical artefacts around the jump. Also, from a modelling point of view, it does not make a lot of sense to model subsurface topology by periodic base functions. See figure 2.3 for a demonstration of this phenomenon.

An alternative approach is given by priors which are given by randomized weighted series of different base functions than trigonometric polynomials. One possibility is the employment of orthonormal wavelets. This leads to a *localized* orthonormal decomposition of functions. If we use wavelets which are able to model jumps, we can even reproduce sharp interfaces.

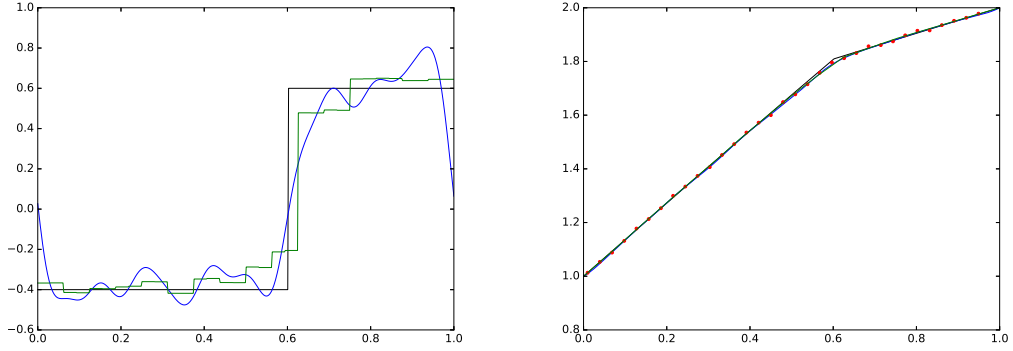


Figure 1: Comparison of trigonometric and wavelet prior for a 1d inverse elliptical problem. Right: Pressure with observations. Left: Ground truth permeability (black piecewise constant with values  $-0.4$  and  $0.6$ ), MAP point for  $(-\Delta)^{-1}$  prior (blue “wiggly” line) and MAP point for wavelet prior (green piecewise constant curve with many jumps)

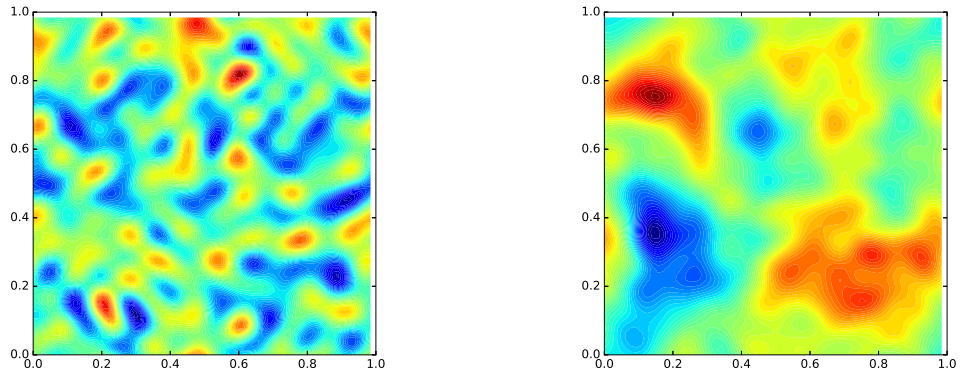


Figure 2: Samples from a  $N(0, (-\Delta)^{-\alpha})$  prior (left:  $\alpha = 1.0$ , right:  $\alpha = 2.5$ )

### 3 (Haar) wavelets and wavelet priors

The first wavelet was the Haar wavelet, conceived by Alfred Haar [28] as a method of generating an unconditional basis for  $L^2([0, 1])$  (the Haar wavelet in fact builds an unconditional basis also for general  $L^p$  spaces). Wavelets really took off in the 70s and 80s with notably Ingrid Daubechies' description of compactly supported continuous wavelets [15] (the Haar wavelet is discontinuous) and Stéphane Mallat's general framework of multiresolution analysis [36]. A classical introduction are Daubechies' marvelous "ten lectures" [16], a very instructive and readable account is by Blatter [4]. In the following, we will only use Haar's original wavelets. The discontinuity (which can be a disadvantage for some applications e.g. in image processing) is actually a favorable property in our case as we want to model sharp interfaces in subsurface topology and thus we do not need or want more sophisticated wavelets (at least for the purpose of this study).

#### 3.1 Haar wavelet expansions of functions on $[0, 1]^d$

We will work with dimension one and two; the step to higher dimensions is straightforward (although computationally challenging!).

##### 3.1.1 Dimension one

Define the Haar scale function and Haar mother wavelet in 1d by

$$\phi(x) = \mathbb{1}_{[0,1)}(x), \quad \psi(x) = \mathbb{1}_{[0, \frac{1}{2})}(x) - \mathbb{1}_{[\frac{1}{2}, 1)}(x),$$

where  $\mathbb{1}_A(x) = 1$  if  $x \in A$  and  $\mathbb{1}_A(x) = 0$  else. The scaled wavelets are

$$\psi_{j,k}(x) = 2^{j/2} \cdot \psi(2^j x - k).$$

We know that we can write any  $f \in L^2[0, 1]$  as

$$f(x) = w_0 \cdot \phi(x) + \sum_{j=0}^{\infty} \sum_{k=0}^{2^j-1} w_{j,k} \cdot \psi_{j,k}(x) \tag{5}$$

$$= w_0 \cdot \phi(x) + \sum_{l=1}^{\infty} c_l \psi_l(x) \tag{6}$$

where the second line is a re-indexing of  $(j, k) \mapsto l(j, k) = 2^j + k$  and  $\psi_l = \psi_{j,k}$  for the appropriate change of index (see figure 3.1.1). The justification for this to work is multiresolutional analysis (see [16]), but the main point is that wavelets give a way to give a *local* way of spanning functions (as compared to, say, trigonometric polynomials – the exact opposite of local) which is also *robust with respect to fine discretization* (as opposed to a naive spanning of a function by evaluating it on a grid). We show how the wavelet expansion is computed for a concrete function: Let  $f$  be given by its values on a uniform grid of  $[0, 1]$ . We always assume that the number of grid points is a power of 2, i.e.  $\vec{f} = (f(0), f(2^{-N}), \dots, f(1 - 2^{-N}))^T$ . Now we define  $a_N^{(k)} := f(k \cdot 2^{-N})$ . The iteratively

$l$	$j$	$k$
1	0	0
2, 3	1	0, 1
$\vdots$	$\vdots$	
$2^i, \dots, 2^{i+1} - 1$	$i$	$0, \dots, 2^i - 1$

Figure 3: Index table for dimension one

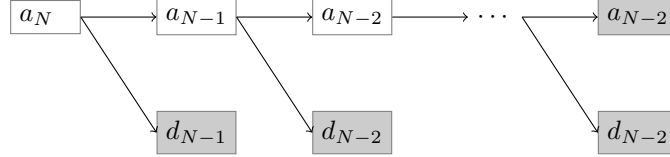


Figure 4: Expansion calculation. Filled nodes represent quantities directly used for the expansion.

we compute

$$a_j^{(k)} := \frac{a_{j+1}^{(2k)} + a_{j+1}^{(2k+1)}}{2}$$

$$d_j^{(k)} := \frac{a_{j+1}^{(2k)} - a_{j+1}^{(2k+1)}}{2}$$

for  $j = 0, \dots, N - 1$  and  $k = 0, \dots, 2^n - 1$ , i.e. every step  $j \mapsto j + 1$  halves the size of the vectors  $a_n$  and  $d_n$  (by coarsening the resolution by a factor of two). Note that we can forget now all  $a_j$  for  $j > 0$ , as  $a_{j+1}^{(2k)} = a_n^{(j)} + d_n^{(k)}$  and  $a_{j+1}^{(2k+1)} = a_n^{(j)} - d_n^{(k)}$ . Then the wavelet expansion is given by the form

$$w_0 \cdot \phi(x) + \sum_{j=0}^{N-1} \sum_{k=0}^{2^j-1} w_{j,k} \cdot \psi_{j,k}(x)$$

with  $w_0 = a_0$  and  $w_{j,k} = d_j^{(k)}$ . Note that the sum is finite as having started with values of  $f$  on a grid puts a lid on the maximal resolution.

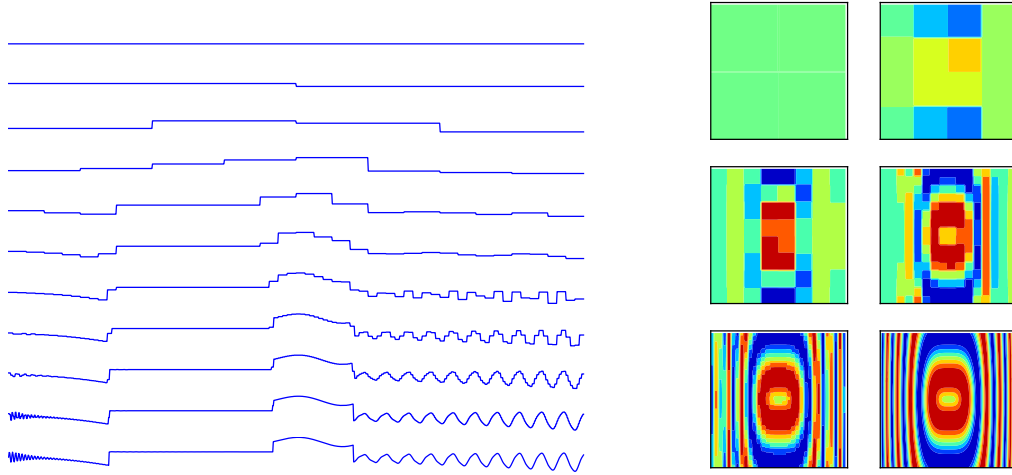


Figure 5: Left: Reconstruction of a one-dimensional function from its wavelet decomposition:  $\ell$ -th row shows  $a_0 \cdot \phi(x) + \sum_{j=0}^{\ell-1} \sum_{k=0}^{2^j-1} d_j^{(k)} \cdot \psi_{j,k}(x)$ . Right: Reconstruction of a two-dimensional function from its wavelet decomposition.

### 3.1.2 Dimension two

Here we need to define the scale function and three mother wavelets.

$$\begin{aligned} \phi(x, y) &= \phi(x) \cdot \phi(y) \\ &= \mathbb{1}_{[0,1]^2}(x, y) \end{aligned}$$

$$\begin{aligned} \psi^{(0)}(x, y) &= \phi(x) \cdot \psi(y) \\ &= \mathbb{1}_{[0,1] \times [0,1/2)}(x, y) - \mathbb{1}_{[0,1] \times [1/2,1)}(x, y) \end{aligned}$$

$$\begin{aligned} \psi^{(1)}(x, y) &= \psi(x) \cdot \phi(y) \\ &= \mathbb{1}_{[0,1/2) \times [0,1)}(x, y) - \mathbb{1}_{[1/2,1) \times [0,1)}(x, y) \end{aligned}$$

$$\begin{aligned} \psi^{(2)}(x, y) &= \psi(x) \cdot \psi(y) \\ &= \mathbb{1}_{[0,1/2) \times [0,1/2)}(x, y) - \mathbb{1}_{[0,1/2) \times [1/2,1)}(x, y) \\ &\quad - \mathbb{1}_{[1/2,1) \times [0,1/2)}(x, y) + \mathbb{1}_{[1/2,1) \times [1/2,1)}(x, y) \end{aligned}$$

and scaled wavelets

$$\psi_{j,k,n}^{(m)} = 2^j \cdot \psi^m(2^j - k, 2^j - n).$$

$l$	$j$	$m$	$k$	$n$
1	0	0	0	0
2	0	1	0	0
3	0	2	0	0
4, ... 7	1	0	0, 1	0, 1
8, ... 11	1	1	0, 1	0, 1
12, ... 15	1	2	0, 1	0, 1
16, ... 31	2	0	0, ... 3	0, ... 3
32, ... 47	2	1	0, ... 3	0, ... 3
48, ... 63	2	2	0, ... 3	0, ... 3
$4^i, \dots 2 \cdot 4^i - 1$	$i$	0	$0, \dots 2^i - 1$	$0, \dots 2^i - 1$
$2 \cdot 4^i, \dots 3 \cdot 4^i - 1$	$i$	1	$0, \dots 2^i - 1$	$0, \dots 2^i - 1$
$3 \cdot 4^i, \dots 4^{i+1} - 1$	$i$	2	$0, \dots 2^i - 1$	$0, \dots 2^i - 1$

Figure 6: Index table for dimension two

With this we can expand a function defined on  $[0, 1]^2$  by

$$\begin{aligned}
f(x, y) &= w_0 \cdot \phi(x, y) + \sum_{j=0}^{\infty} \sum_{m=0}^2 \sum_{k=0}^{2^j-1} \sum_{n=0}^{2^j-1} w_{j,k,n}^{(m)} \cdot \psi_{j,k,n}^{(m)}(x, y) \\
&= w_0 \cdot \phi(x, y) + \sum_{l=1}^{\infty} c_l \psi_l(x, y)
\end{aligned}$$

where as in 1d we re-index  $(j, m, k, n) \mapsto l(j, m, k, n) = 4^j + m \cdot 4^j + k \cdot 2^j + l$  or as in the table in figure 3.1.2. Calculation of the wavelet expansion in two dimension is done as follows:

Given a function by its values on a square, power-of-4 grid  $\{0, 2^{-N}, \dots, 1 - 2^{-N}\}^2$  we define  $a_N^{(k,n)} = f(k \cdot 2^{-N}, n \cdot 2^{-N})$  and

$$\begin{aligned}
a_j^{(k,n)} &:= \frac{a_{j+1}^{(2k,2n)} + a_{j+1}^{(2k+1,2n)} + a_{j+1}^{(2k,2n+1)} + a_{j+1}^{(2k+1,2n+1)}}{4} \\
d_j^{0,(k,n)} &:= \frac{a_{j+1}^{(2k,2n)} + a_{j+1}^{(2k+1,2n)} - a_{j+1}^{(2k,2n+1)} - a_{j+1}^{(2k+1,2n+1)}}{4} \\
d_j^{1,(k,n)} &:= \frac{a_{j+1}^{(2k,2n)} - a_{j+1}^{(2k+1,2n)} + a_{j+1}^{(2k,2n+1)} - a_{j+1}^{(2k+1,2n+1)}}{4} \\
d_j^{2,(k,n)} &:= \frac{a_{j+1}^{(2k,2n)} - a_{j+1}^{(2k+1,2n)} - a_{j+1}^{(2k,2n+1)} + a_{j+1}^{(2k+1,2n+1)}}{4}
\end{aligned}$$

and analogously to one dimension, we can then span  $f$  by

$$a_0 \cdot \phi(x, y) + \sum_{j=0}^{N-1} \sum_{m=0}^2 \sum_{k=0}^{2^j-1} \sum_{n=0}^{2^j-1} d_j^{m,(k,n)} \cdot \psi_{j,k,n}^{(m)}(x, y)$$

where the meaning of the indices is as follows:

- $j$ : Scale
- $m$ : Orientation (0=Horizontal, 1=Vertical, 2=Diagonal)
- $k$ : Shift in horizontal direction
- $n$ : Shift in vertical direction

### 3.1.3 Arbitrary dimension

Just for reference we give the straight-forward extension to arbitrary dimension  $d \in \mathbb{N}$ : Given a function  $f : [0, 1]^d \rightarrow \mathbb{R}$ , we define  $\Lambda = \{0, \dots, 2^j - 1\}^d$  and span

$$f(z) = w_0 \cdot \phi(z) + \sum_{j=0}^{\infty} \sum_{m=0}^{2^d-1} \sum_{k \in \Lambda} w_{j,k}^{(m)} \cdot \psi_{j,k}^{(m)}(z)$$

## 3.2 Wavelets and Besov spaces

We can characterize (see [49], [16], [38], and in the context of inverse problems, [7] (for  $d = 1$ ), [12] (with characterization (7), in their notation  $X^{s,q} = B_{qq}^s$ ), and also [32], [34]) elements of Besov space  $B_{pp}^s$  by the following: Let  $f : [0, 1]^d \rightarrow \mathbb{R}$ . Assume that the wavelet basis used is regular enough. Then for  $p > 0$  and  $s \in \mathbb{R}$ ,

$$f \in B_{pp}^s([0, 1]^d) \Leftrightarrow \left( \sum_{l=1}^{\infty} l^{\frac{ps}{d} + \frac{p}{2} - 1} \cdot |c_l|^p \right)^{\frac{1}{p}} < \infty. \quad (7)$$

In one and two dimensions this reduces to the following:

$$\begin{aligned} f \in B_{pp}^s([0, 1]), d = 1 \\ \Leftrightarrow \|f\|_{B_{pp}^s} := \left( |w_0|^p + \sum_{j=0}^{\infty} 2^{jp(s + \frac{1}{2} - \frac{1}{p})} \cdot \sum_{k=0}^{2^j-1} |w_{j,k}|^p \right)^{\frac{1}{p}} < \infty \end{aligned} \quad (8)$$

$$\begin{aligned} f \in B_{pp}^s([0, 1]^2), d = 2 \\ \Leftrightarrow \|f\|_{B_{pp}^s} := \left( |w_0|^p + \sum_{j=0}^{\infty} 2^{jp(s + 1 - \frac{2}{p})} \cdot \sum_{m=0}^2 \sum_{k=0}^{2^j-1} \sum_{n=0}^{2^j-1} |w_{j,k,n}^{(m)}|^p \right)^{\frac{1}{p}} < \infty. \end{aligned} \quad (9)$$

Note that the formula in (7) does not yield the same numerical value as the appropriate dimension-dependent formula for  $\|f\|_{B_{pp}^s}$  but that the expressions are merely equivalent in the sense of equivalent norms.

If we set  $p = 2$ , we recover the Sobolev spaces, i.e.  $B_{2,2}^s = H^s$ .

**Remark 1.** Note that Besov spaces usually have an additional parameter, i.e.  $B_{p,q}^s$  although we only use the case  $p = q$  for our choice of priors. For completeness, (both for general  $p > 0, q > 0, s \in \mathbb{R}$

and dimension  $d$ ) the  $B_{p,q}^s$  Besov norm for functions defined on  $[0, 1]^d$  is defined by

$$\|f\|_{B_{p,q}^s([0,1]^d)} := \left( |w_0|^p + \sum_{j=0}^{\infty} 2^{jq(s+\frac{d}{2}-\frac{d}{p})} \left( \sum_{m=0}^{2^d-1} \sum_{k \in \Lambda} |w_{j,k}^{(m)}|^p \right)^{\frac{q}{p}} \right)^{\frac{1}{q}}$$

### 3.3 Wavelet (“Besov”) priors

We can construct a probability measure on Besov spaces (i.e. we define random Besov functions) by randomizing coefficients in the wavelet expansion in a suitable way. To this end, we set  $\xi_l \sim \exp(-|x|^p/2)$  (i.e. for  $p = 2$  these are normal random variables, for  $p = 1$  we have Laplace samples etc.). Furthermore we define an inverse scale parameter  $\kappa$  and set  $t \geq 0$ . Then in dimension  $d$  we can define a random function on  $[0, 1]^d$  by setting

$$u(x) = \sum_{l=1}^{\infty} l^{-(\frac{t}{d}+\frac{1}{2}-\frac{1}{p})} \cdot \kappa^{-1/p} \cdot \xi_l \cdot \psi_l(x).$$

This is the notation in [34], [12], which is very suitable for proving various regularity results but not very natural from an implementation point of view. To see this, note that the enumeration of  $j, k$  (the resolution and shift parameter) by just one index  $l$  and the scaling of the coefficients by  $l^{-(\frac{t}{d}+\frac{1}{2}-\frac{1}{p})}$  leads to a spatially inhomogeneous span of random functions. We follow the notation in [32], [7], which stems from the form of equations (8) and (9) and differentiate by dimension.

**1D** Set  $\xi_{j,k} \sim \exp(-|x|^p/2)$  i.i.d. Then

$$v(x) = \kappa^{-1/p} \cdot \sum_{j=0}^{\infty} 2^{-j(t+\frac{1}{2}-\frac{1}{p})} \sum_{k=0}^{2^j-1} \xi_{j,k} \cdot \psi_{j,k}(x)$$

is a random function defined on  $[0, 1]$ .

**2D** Set  $\xi_{j,k,n}^{(m)} \sim \exp(-|x|^p/2)$  i.i.d. Then

$$v(x, y) = \kappa^{-1/p} \cdot \sum_{j=0}^{\infty} 4^{-j(\frac{t}{2}+\frac{1}{2}-\frac{1}{p})} \sum_{m=0}^2 \sum_{k=0}^{2^j-1} \sum_{n=0}^{2^j-1} \xi_{j,k,n}^{(m)} \cdot \psi_{j,k,n}^{(m)}(x, y)$$

is a random function defined on  $[0, 1] \times [0, 1]$ . In either dimension, we call such a random function a sample from a  $(\kappa, B_{pp}^s)$  Wavelet prior.

For convenience, we record the following regularity result:

**Lemma 1** (from [34], modification with  $\kappa$  from [12]). *Let  $\kappa > 0, p \geq 1, s > 0$  and  $v$  a sample from a  $(\kappa, B_{pp}^s)$  Wavelet prior as above. The following conditions are equivalent:*

- $\|v\|_{B_{pp}^t} < \infty$  almost surely.
- $\mathbb{E} \exp(\alpha \|v\|_{B_{pp}^t}^p) < \infty$  for any  $\alpha \in (0, \kappa/2)$ .

- $t < s - d/p$ .

Note that in particular, a sample from a  $(\kappa, B_{pp}^s)$  Wavelet prior will in general *not* have finite  $B_{pp}^s$  norm!

In the case  $p = 2$ , we obtain a Wavelet-based Gaussian prior with mean 0 and covariance operator  $C$  with property

$$C\psi_{j,k,n}^{(m)} = \kappa^{-1} \cdot 4^{-js} \psi_{j,k,n}^{(m)},$$

i.e. we can think of the prior as being a diagonal Gaussian over all Wavelets with exponential decay governed by  $s$  and length scale given by  $\kappa^{-1}$ . In this case the Cameron–Martin space is  $E = B_{22}^s = H^s$  (which is the space giving its name to the measure) and with Cameron–Martin norm given by  $\|\cdot\|_E = \|\cdot\|_{B_{22}^s}$ . In this case, the Cameron–Martin norm generates an inner product by

$$\langle u, v \rangle_E = \sum_{j=0}^{\infty} 4^{js} \cdot \sum_{k=0}^{2^j-1} w_{j,k}(u) \cdot w_{j,k}(v)$$

in dimension one (where  $w_{j,k}(u)$  is the Wavelet decomposition coefficient of  $u$  and likewise for  $w_{j,k}(v)$ ). In dimension two,

$$\langle u, v \rangle_E = \sum_{j=0}^{\infty} 4^{js} \cdot \sum_{m=0}^2 \sum_{k=0}^{2^j-1} \sum_{n=0}^{2^j-1} w_{j,k,n}^{(m)}(u) \cdot w_{j,k,n}^{(m)}(v)$$

In the case  $p \neq 2$  we define  $\|\cdot\|_E = \|\cdot\|_{B_{pp}^s}$  nevertheless. In the “proper” Besov case (i.e. non-Gaussian),  $E$  is not a Hilbert space (and not the Cameron–Martin space which is only defined for Gaussians), but has the similar defining property of being the space of admissible shifts. For a proof of this, consult [1, Lemma 3.5], see also [29].

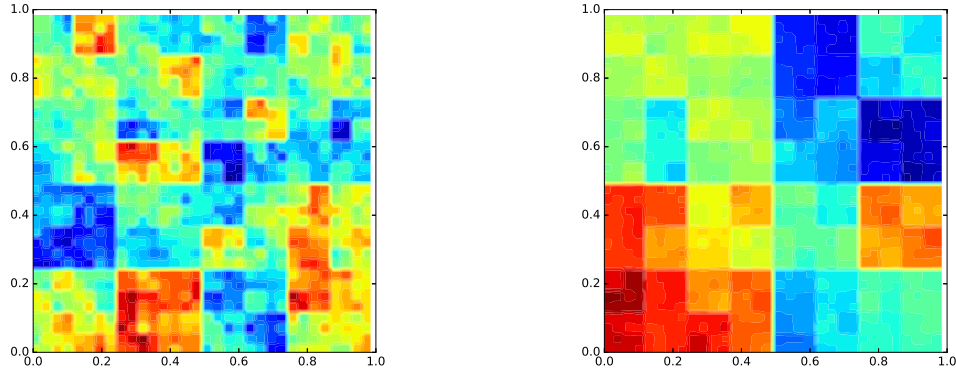


Figure 7: Samples from a  $(0.1, B_{22}^s)$  prior (left:  $s = 1.0$ , right:  $s = 2.0$ )

### 3.4 A remark on the name “Besov prior”

Note that the notion of randomizing a wavelet expansion in the context of Bayesian inverse problems has been called Besov priors, most notably by [34], [12], [32]. In this paper, the name “Wavelet prior” is preferred, for several reasons:

- If the prior is a Gaussian prior (i.e.,  $p = 2$ ), the  $B_{pp}^s$  Besov prior (in the convention of the references above) is named after its Cameron-Martin space and in particular, samples of  $B_{pp}^s$  will with probability one *not* lie in  $B_{pp}^s$ , which can lead to some confusion.
- Strictly speaking, in order to construct a  $B_{pp}^s$  Besov prior, we need to start with a  $\psi, \phi$  pair which is at least  $s$ -regular. A function  $f$  is  $s$ -regular, if  $f \in C^s$  and  $|\partial^\alpha f(x)| \leq C_m(1 + |x|)^{-m}$  for all  $m \in \mathbb{N}$  and  $|\alpha| \leq s$ . Our choice of  $\phi$  and  $\psi$  is not even continuous (but still leads to an interesting prior).
- From an applied modelling point of view, the fact that “plausible” parameters (as defined by the prior) are spanned by a certain class of wavelets (as opposed to trigonometric functions) is more strongly defining feature than its approximation property of some function space.

To summarize, in this context, “Wavelet prior” means some sort of randomized wavelet expansion which is well-defined in the limit of arbitrarily fine spatial discretization.

## 4 Finding the maximum a posteriori point

Although the construction of the inverse problem was motivated from a Bayesian viewpoint, we will concentrate on obtaining the MAP (maximum a posteriori) reconstruction from the data, as opposed to sampling from the full posterior. This is something that should be done in a subsequent study, although our focus on the MAP estimator can be motivated from the small noise setting: Here we assume that the observations are very close to the truth and thus there is very little variation in samples from the posterior and the MAP estimator is a characteristic quantity.

The techniques in this section (i.e. using the adjoint approach to calculate quantities of interest) are fairly standard (see for example [26], [27]). We record them here briefly as in the wavelet setting there is a slight twist which speeds up the computation immensely. Recall that (write  $z = (x, y)$ )

$$\begin{aligned} -\nabla \cdot (e^{u(z)} \cdot \nabla p_u(z)) &= f(z) \text{ in } [0, 1]^2 \\ p(z) &= g(z) \text{ on } \Gamma_D \\ \partial_\nu p(z) &= h(z) \text{ on } \Gamma_N \end{aligned}$$

Note that we now record the  $u$ -dependence of the solution of the PDE explicitly by writing  $p_u$ .

We first need to find a  $G \in H^1(\Omega)$ , such that  $\text{trace}(G) = g$  and then we define  $P_u := p_u - G$ . Then the PDE for  $P_u$  is

$$\begin{aligned} -\nabla \cdot (e^{u(z)} \cdot \nabla P_u(z)) &= f(z) + \nabla \cdot (e^{u(z)} \cdot \nabla G(z)), \quad \text{in } [0, 1]^2 \\ P_u(z) &= 0, \quad \text{on } \Gamma_D \\ \partial_\nu P_u(z) &= h(z) - \partial_\nu G(z), \quad \text{on } \Gamma_N. \end{aligned}$$

A good space of test functions is  $H_{0,D}^1 := \{\phi \in H^1(\Omega) : \text{trace}(\phi) = 0 \text{ on } \Gamma_D\}$ . Now this has a variational form: We call  $P_u \in H_{0,D}^1$  the solution of the PDE, if  $P_u = P$  is the unique solution of

$$\int_{\Omega} e^u \cdot \nabla P \cdot \nabla \phi = \int_{\Omega} f \phi - \int_{\Omega} e^u \cdot \nabla \phi \cdot \nabla G + \int_{\Gamma_N} h \text{trace}(\phi) \quad \text{for all } \phi \in H_{0,D}^1.$$

Then  $p_u = P_u + G$  is the solution of the original PDE. We can write that  $p_u \in H_{g,D}^1 := \{\phi \in H^1(\Omega) : \text{trace}(\phi) = g \text{ on } \Gamma_D\}$

#### 4.1 Calculating sensitivities of a quantity of interest with respect to parameter variation

We have a quantity of interest<sup>3</sup> depending on the solution to our original PDE,  $q : H_{g,D}^1 \rightarrow \mathbb{R}$ , and we are interested in the sensitivity of  $q(p_u)$  on the parameter scalar field  $u$ .

For this to work we define the implicit dependence of  $u$  and  $p_u$  by the following expression:  $p_u$  is the unique (by PDE theory)  $p \in H_{g,D}^1$  such that

$$0 = J(u, p) = -\nabla \cdot (e^u \cdot \nabla p) - f.$$

The implicit function theorem yields the existence of a function  $\mathbf{p} : L^\infty \rightarrow H_{g,D}^1$  with  $J(u, \mathbf{p}(u)) = 0$  and  $D_u \mathbf{p}(\bar{u}) = [D_p J(\bar{u}, \mathbf{p}(\bar{u}))]^{-1} \circ D_u J(\bar{u}, \mathbf{p}(\bar{u}))$ . Then our quantity of interest can be written as a function of  $u$ .<sup>4</sup>

$$Q(u) := q(p_u) = q(\mathbf{p}(u)).$$

We can calculate the mentioned sensitivity by evaluating the Fréchet derivative

$$D_u Q(\bar{u}) = D_p q(p_{\bar{u}}) \circ D_u \mathbf{p}(\bar{u}) = D_p q(p_{\bar{u}}) \circ [D_p J(\bar{u}, \mathbf{p}(\bar{u}))]^{-1} \circ D_u J(\bar{u}, \mathbf{p}(\bar{u})) \quad (10)$$

$$D_u Q(\bar{u})[\varphi] = D_p q(p_{\bar{u}}) \{ [D_p J(\bar{u}, p_{\bar{u}})]^{-1} (D_u J(\bar{u}, p_{\bar{u}})[\varphi]) \} \quad (11)$$

Now we use the special structure of  $J$ :

$$D_u J(\bar{u}, p_{\bar{u}})[\varphi] = -\nabla \cdot (\varphi \cdot e^{\bar{u}} \cdot \nabla p_{\bar{u}})$$

$$D_p J(\bar{u}, p_{\bar{u}})[v] = -\nabla \cdot (e^{\bar{u}} \cdot \nabla v)$$

and hence

$$w = [D_p J(\bar{u}, p_{\bar{u}})]^{-1} (D_u J(\bar{u}, p_{\bar{u}})[\varphi])$$

is the unique element  $w$  given by the PDE

$$\begin{aligned} -\nabla \cdot (e^{\bar{u}} \cdot \nabla w) &= -\nabla \cdot (\varphi \cdot e^{\bar{u}} \cdot \nabla p_{\bar{u}}) \\ w &= 0 \text{ on } \Gamma_D \\ \partial_\nu w &= 0 \text{ on } \Gamma_N. \end{aligned} \quad (12)$$

<sup>3</sup>This section closely follows [46]. Thanks to Donald Estep for explaining to me how to obtain the adjoint PDE with inhomogenous boundary conditions, see also [22].

<sup>4</sup>We will use  $p_u$  and  $\mathbf{p}(u)$  interchangeably depending on whether we view it as a  $H_{g,D}^1$  object or whether we focus on the explicit  $u$ -dependence coming from the implicit function theorem

The boundary conditions on  $w$  arise from the fact that  $D_u J(\bar{\theta}, u_{\bar{\theta}}) : H_{0,D}^1 \rightarrow \mathbb{R}$  because  $H_{0,D}^1$  is the “difference space” of  $H_{g,D}^1$ . Combining this with (11), we can express  $D_u Q(\bar{u})[\varphi]$  as follows:

$$D_u Q(\bar{u})[\varphi] = D_p q(p_{\bar{u}})[w],$$

which is a linear functional acting on  $w$ . Now if we are interested in the gradient of  $Q(\bar{\theta})$ , there is a straightforward way to do this by calculating  $D_{\theta} Q(\bar{\theta})[\varphi]$  for “all” directions  $\varphi$  and concluding this in a column vector which then is the gradient. This entails solving the PDE on  $w$  as many times as we have directions  $\varphi$ , which can be prohibitively costly. By the adjoint method, we have a more clever way.

#### 4.1.1 Evaluating linear functionals of solutions of 2nd order PDEs with the adjoint method

We consider a second-order elliptical PDE of the form

$$\begin{aligned} -\nabla \cdot (e^u \cdot \nabla v) &= f \text{ in } \Omega \\ v &= g \text{ on } \Gamma_D \\ \partial_{\nu} v &= h \text{ on } \Gamma_N \end{aligned}$$

for  $f \in H^{-1}$ ,  $\Gamma_D \cup \Gamma_N = \partial\Omega$  and we are interested in the value of

$$\int_{\Omega} \ell \cdot v,$$

where  $\ell \in H^{-1}$ . Now this is equivalent to evaluating

$$\int_{\Omega} f \cdot \tilde{v} - \int_{\Gamma_D} g \cdot e^{\theta} \cdot \partial_{\nu} \tilde{v} + \int_{\Gamma_N} h \cdot e^{\theta} \cdot \tilde{v},$$

where

$$\begin{aligned} -\nabla \cdot (e^u \cdot \nabla \tilde{v}) &= l \text{ in } \Omega \\ \tilde{v} &= 0 \text{ on } \Gamma_D \\ \partial_{\nu} \tilde{v} &= 0 \text{ on } \Gamma_N \end{aligned}$$

as can be shown easily by partially integrating twice.

## 4.2 Calculating sensitivities of a quantity of interest with respect to parameter variation (continued)

As

$$D_u Q(\bar{u})[\varphi] = D_p q(p_{\bar{u}})[w]$$

is a linear functional acting on  $w$ , we are exactly in the setting of the last section.

We know that we can evaluate this quantity by working with the adjoint PDE for  $w$  which is

$$\begin{aligned} -\nabla \cdot (e^{\bar{u}} \cdot \nabla \tilde{w}) &= D_p q(p_{\bar{u}}) \text{ in } [0, 1]^2 \\ \tilde{w} &= 0 \text{ on } \Gamma_D \\ \partial_{\nu} \tilde{w} &= 0 \text{ on } \Gamma_N. \end{aligned} \tag{13}$$

This is just one PDE which we need to solve and now we just need to evaluate the inner product of  $\tilde{w}$  with the primal PDE's (12) right hand side

$$\int_{\Omega} -\nabla \cdot (\varphi e^{\bar{u}} \cdot \nabla p_{\bar{u}}) \cdot \tilde{w} = \int_{\Omega} \varphi \cdot e^{\bar{u}} \cdot \nabla p_{\bar{u}} \cdot \nabla \tilde{w}$$

for each direction  $\varphi$  and this will be  $D_u Q(\bar{u})[\varphi]$ . In the case that our parameter space is spanned by a Wavelet basis and we are interested in the sensitivity in direction  $\phi$ , where  $\phi$  is an element of our wavelet basis, the inner product is actually the computation of the wavelet decomposition of  $e^{\bar{u}} \cdot \nabla p_{\bar{u}} \cdot \nabla \tilde{w}$ :

$$\begin{aligned} D_u Q(\bar{u})[\psi_l] &= c_l, \text{ where} \\ e^{\bar{u}} \cdot \nabla p_{\bar{u}} \cdot \nabla \tilde{w} &= \sum_{l=1}^{\infty} c_l \cdot \psi_l \end{aligned}$$

is a Wavelet decomposition and  $\tilde{w}$  is the solution of (13).

For a wavelet resolution of  $2^J \times 2^J$  we have  $4^J$  "directions", i.e.  $4^J$  entries in the gradient. This means we have diminished our computational effort for computing the gradient from  $4^J$  PDE solves to 2 PDE solves (one solve for  $p_{\bar{u}}$  and one solve for  $\tilde{w}$  which depends on  $p_{\bar{u}}$ ) and one wavelet decomposition calculation, which in general is a huge improvement.

### 4.3 Sensitivity of a data misfit functional

Consider the case of

$$q(p) = \Phi(p) = \frac{1}{2\gamma^2} \|y - \Pi p\|^2$$

in the setting of section 2.2. Its Fréchet derivative is  $D_p q(p_{\bar{u}})(w) = -\frac{1}{\gamma^2} \cdot \langle y - \Pi p_{\bar{u}}, \Pi w \rangle$  and we can write  $D_p q(p_{\bar{u}}) \in H^{-1}$  by

$$D_p q(p_{\bar{u}}) = -\frac{1}{\gamma^2} \cdot \sum_{i=1}^N (y_i - p_{\bar{u}}(x_i)) \cdot \delta_{x_i}$$

and hence we can compute the sensitivity w.r.t. the parameter  $u$  by the following two-step procedure:

**Algorithm 1** (Computing the QoI's gradient).

1. Compute the solution  $\tilde{w}$  of

$$\begin{aligned} -\nabla \cdot (e^{\bar{u}} \cdot \nabla \tilde{w}) &= -\frac{1}{\gamma^2} \cdot \sum_{i=1}^N (y_i - p_{\bar{u}}(x_i)) \cdot \delta_{(x_i)} \\ \tilde{w} &= 0 \text{ on } \Gamma_D \\ \partial_\nu \tilde{w} &= 0 \text{ on } \Gamma_N. \end{aligned}$$

2. Obtain the wavelet expansion of  $e^{\bar{u}} \cdot \nabla p_{\bar{u}} \cdot \nabla \tilde{w}$  in the form

$$e^{\bar{u}} \cdot \nabla p_{\bar{u}} \cdot \nabla \tilde{w} = \sum_{l=1}^{\infty} c_l \cdot \psi_l$$

(either by computing  $c_l = \int_{\Omega} \psi_l \cdot e^{\bar{u}} \cdot \nabla p_{\bar{u}} \cdot \nabla \tilde{w}$  or by a fast wavelet transformation on a grid). Then  $D_u Q(\bar{u})(\psi_l) = c_l$ , or

$$\nabla_u Q(\bar{u}) = (c_l)_{l \in \mathbb{N}}.$$

**Remark 2.** The last step is where the choice of wavelets really pays off: The solution  $\tilde{w}$  of the dual PDE encodes the gradient information and entries of the gradient vector can be calculated by computing the projection of  $e^{\bar{u}} \cdot \nabla p_{\bar{u}} \cdot \nabla \tilde{w}$  onto the elements of the basis used (in this case: wavelet functions). This is easily approximated for the choice of a wavelet basis by constructing the wavelet decomposition of said function. If we take trigonometric functions, this approximation is a lot worse due to the non-periodicity of  $e^{\bar{u}} \cdot \nabla p_{\bar{u}} \cdot \nabla \tilde{w}$ : In this case we cannot use the fast Fourier transform to obtain the entries of the gradient vector and thus we have no fast way of evaluating the gradient.

## 4.4 Computing the MAP point

Now that everything is in place, computing the MAP point consists of solving the optimization problem

$$u_{\text{MAP}} = \operatorname{arginf} I(u) = \operatorname{arginf} \Phi(u) + \frac{1}{2} \|u\|_E^2$$

with  $\|\cdot\|_E$  defined as in section 3.3. We will concentrate on the Gaussian case  $p = 2$  where the role of  $E$  as the Cameron–Martin space of the prior is well-known.

This can be done with a standard BFGS method, for which we need the gradient of  $I$ . After the last section, this is now immediately given by

$$DI(u)[h] = D\Phi(\mathbf{p}(u))[h] + \langle u, h \rangle_E$$

where  $D\Phi(\mathbf{p}(u))[h] = D_u Q(u)[h]$  is calculated as described in section 4.3.

## 5 Simulations

All simulations refer to the elliptical inverse problem from section 2.2. We vary boundary conditions and source terms and in particular various ground truth permeabilities. Forward PDE solving was done with the FEniCS software (see [35], [3]) in python and after calculating the gradient of  $I$  using the technique above, for the optimization procedure for the MAP point we used the scipy optimization implementation of BFGS. The prior used is the  $B_{22}^s$  prior for varying parameters  $s$ . This is not the sparsity-promoting<sup>5</sup> Besov prior  $B_{11}^s$  which is the focus of [7] but rather a proper Gaussian prior.

<sup>5</sup>Note that only the MAP point exhibits sparsity, actual samples from the posterior will in general not be sparse.

## 5.1 Test case 1: simple vertical stripe-shaped topology

- $\Omega = [0, 1] \times [0, 1]$
- $\Gamma_D = \Gamma_{D,1} \cup \Gamma_{D,2} = (\{0\} \times [0, 1]) \cup (\{1\} \times [0, 1])$
- $\Gamma_N = \partial\Omega \setminus \Gamma_D$
- $p = 0$  on  $\Gamma_{D,1}$  and  $p = 2$  on  $\Gamma_{D,2}$ . This specifies  $g$ .
- $\partial_\nu = 0$  on  $\Gamma_N$ . This specifies  $h$ .
- no source terms, i.e.  $f = 0$ .

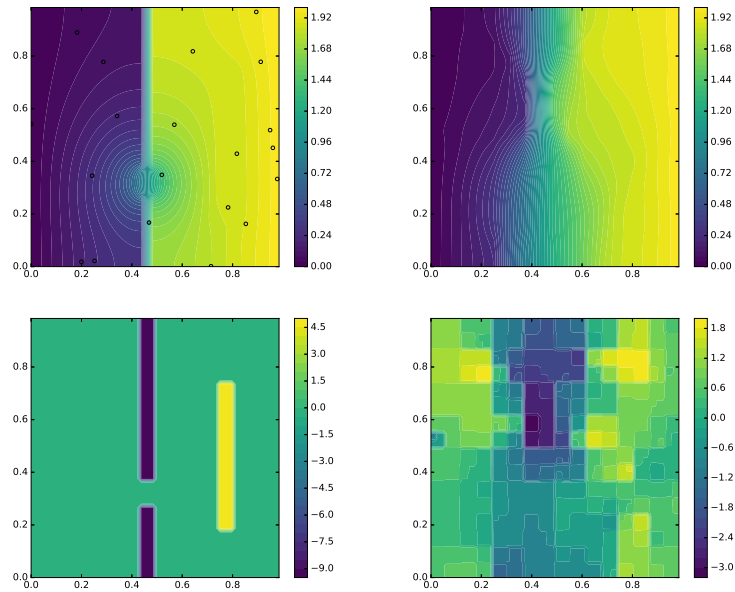


Figure 8: Simulation data for test case 1. Left: Ground truth with observation points ( $\gamma = 0.01$ ,  $N_{obs} = 20$ ). Right:  $u_{\text{MAP}}$  for a  $(0.1, B_{2,2}^{1,5})$  prior with  $J_{\text{max}} = 6$ . Note that the observational positions are not optimally chosen in order to detect the sharp interface.

## 5.2 Test case 2: layered ground truth, different sources

- $\Omega = [0, 1] \times [0, 1]$
- $\Gamma_D = [0, 1] \times \{0\}$

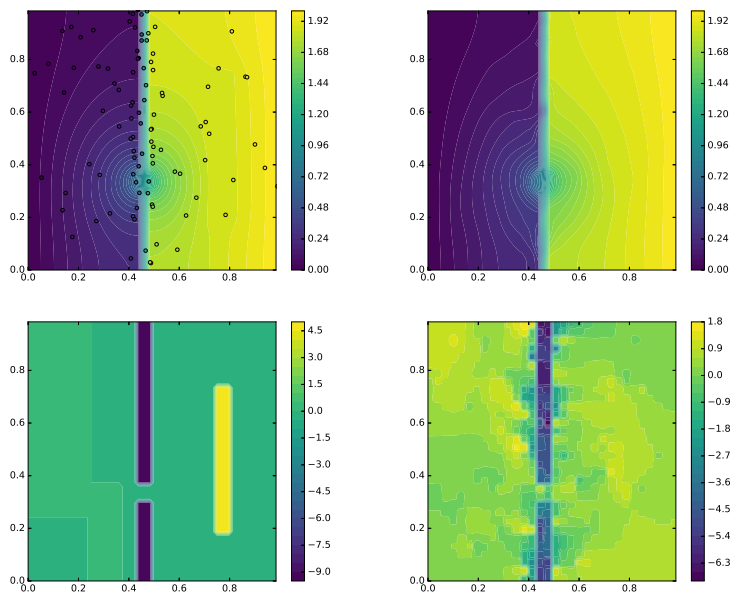


Figure 9: Simulation data for test case 1. Left: Ground truth with observation points ( $\gamma = 0.01$ ,  $N_{obs} = 100$ ). Right:  $u_{MAP}$  for  $(0.1, B_{2,2}^{1,5})$  prior with  $J_{max} = 6$ . The reconstruction is a lot better than in figure 5.1 due to the fact that we have more and better placed observations.

- $\Gamma_N = \partial\Omega \setminus \Gamma_D$
- $p = 0$  on  $\Gamma_D$ . This specifies  $g$ .
- $\partial_\nu p = 0$  on  $\Gamma_N$ . This specifies  $h$ .
- source terms: Varies.

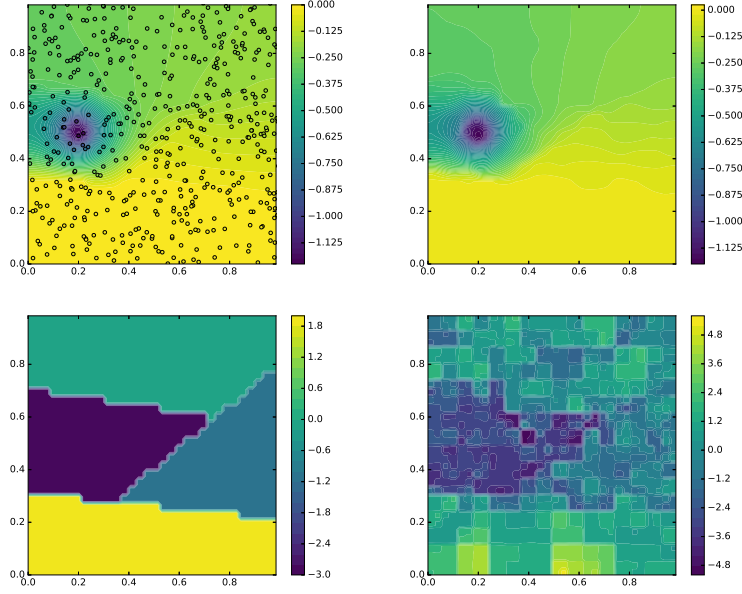


Figure 10: Simulation data for test case 2 with source  $f = -20 \cdot \mathbf{1}_{B_{0.05}(0.2,0.5)}$ . Left: Ground Truth with observation points ( $\gamma = 0.01$ ,  $N_{obs} = 500$ ). Right:  $u_{MAP}$  for a  $(0.1, B_{2,2}^{1.5})$  prior with  $J_{max} = 6$

### 5.3 Test case 3: curved barrier

- $\Omega = [0, 1] \times [0, 1]$
- $\Gamma_D = [0, 1] \times \{0\}$
- $\Gamma_N = \partial\Omega \setminus \Gamma_D$
- $p = 0$  on  $\Gamma_D$ . This specifies  $g$ .
- $\partial_\nu p = 0$  on  $\Gamma_N$ . This specifies  $h$ .
- source terms: Varies.

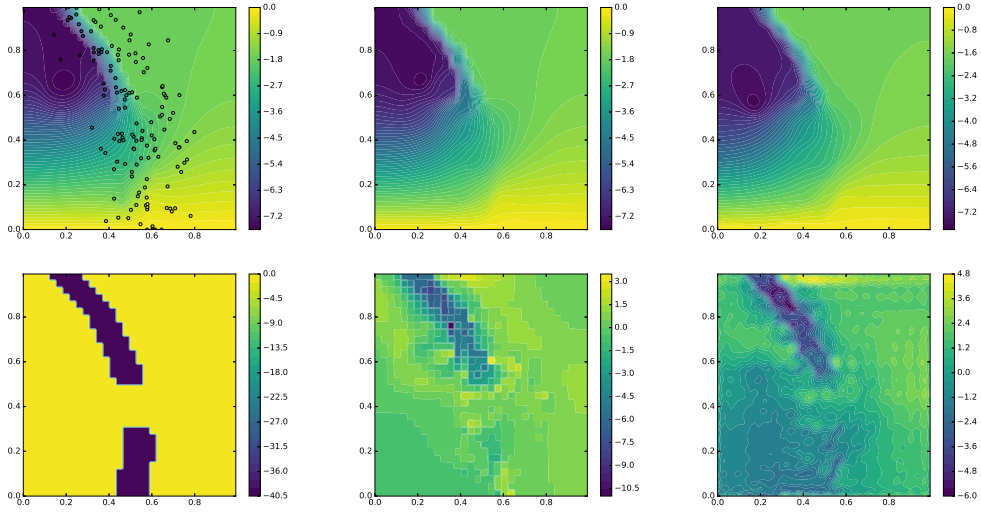


Figure 11: Simulation for test case 3 with source  $f = -200 \cdot \mathbb{1}_{B_{0.05}(0.2,0.6)}$ . Left: Ground truth with observation points ( $\gamma = 0.01$ ,  $N_{obs} = 200$ ). Middle:  $u_{MAP}$  for a  $(0.001, B_{2,2}^{1,0})$  prior with  $J_{max} = 6$ . Right:  $u_{MAP}$  for a  $(-\Delta)^{-1/2}$  prior (trigonometric prior). It is interesting to see that the lower part of the “barrier” cannot be properly resolved as the noise is of a similar order of magnitude as the pressure data in this region.

## 5.4 Comparison between trigonometric and wavelet priors

We record the result of one direct comparison between permeability inference with a trigonometric  $N(0, (-\Delta)^{-\alpha})$  prior and a wavelet-based prior, see figure 5.3.

## 6 Discussion

This paper is supposed to serve as a proof of concept for the implementation of wavelet-based priors in the context of Bayesian inversion. There are many promising modifications possible, some of which will be discussed now and entail “sparse” wavelet priors and spike-and-slab priors. An obvious next step would be to consider a full Bayesian approach by sampling from the posterior instead of calculating just the MAP estimator. Another option would be to discuss the performance of the Ensemble Kalman filter in the wavelet setting, building up on more recent research on this topic, see e.g. [44, 40, 20, 30]

### 6.1 MAP-sparsifying priors

“Sparse” wavelet priors (as used in [7]) refer to  $B_{pp}^s$  priors. Here, the MAP point is the optimizer of an energy functional where the prior-dependent part is sparsity-promoting. As pointed out before, this is the only way in which this prior is sparsifying. This is due to the fact that samples from the Laplace distribution (this is the distribution governing the coefficients of the wavelet decomposition) are almost surely non-zero. In this case, the simulations can be carried out in an equivalent way (although the case  $p > 1$ ,  $p \approx 1$  is easier to handle as the energy functional is differentiable) and the MAP point is seen to be more sparse.

### 6.2 Spike-and-slab priors

Spike-and-slab priors (also called sieve priors) are another story: If we replace the Laplace distributions in the  $B_{1,1}^s$  case by a (possibly weighted) sum of a distribution over the reals (like a Laplace or Gaussian distribution) and a Dirac measure in 0, then samples will be zero with non-zero probability by virtue of the Dirac contribution.<sup>6</sup> In this way one can in principle obtain a sparsifying prior. There is one mathematical challenge and one practical challenge with this choice of prior: It is unclear how to define an equivalent for  $\|\cdot\|_E$  in this setting (with a rigorous justification) and Spike-and-slab priors are notoriously hard to sample from. The non-continuous nature of this prior also yields a non-continuous optimization problem if one is interested in the MAP point. Nevertheless, it would be interesting to pursue this angle.

Another note on sparsity with Wavelets: We remark that “sparse-looking” matrices need not necessarily have a sparse wavelet decomposition:

$$\begin{pmatrix} 2 & 2 & 2 & -2 \\ 2 & 2 & 2 & -2 \\ 2 & 2 & 2 & -2 \\ 2 & 2 & 2 & -2 \end{pmatrix} = \begin{pmatrix} 1 & 1 & 1 & 1 \\ 1 & 1 & 1 & 1 \\ 1 & 1 & 1 & 1 \\ 1 & 1 & 1 & 1 \end{pmatrix} + \begin{pmatrix} 1 & 1 & -1 & -1 \\ 1 & 1 & -1 & -1 \\ 1 & 1 & -1 & -1 \\ 1 & 1 & -1 & -1 \end{pmatrix} + \begin{pmatrix} 0 & 0 & 2 & -2 \\ 0 & 0 & 2 & -2 \\ 0 & 0 & 2 & -2 \\ 0 & 0 & 2 & -2 \end{pmatrix}$$

In this case, a single fault between the third and fourth column needs three non-zero wavelet coefficients to model. This is due to the fact that the interface is not at a “nice” position. In

---

<sup>6</sup>This is something that Youssef Marzouk suggested in a personal conversation.

general, for a  $2^N \times 2^N$  matrix, with a single fault between the  $k$ -th and  $k + 1$ -th column, we need  $B$  non-zero wavelet coefficients where  $B$  is the number of non-zero terms  $a_l$  in the binary decomposition  $k = \sum_{l=0}^{N-1} a_l \cdot 2^l$ , where  $a_l \in \{0, 1\}$ .

In general, one can say that the strongest advantage of Wavelet priors are also what makes them difficult to work with: Every possible function (in the corresponding function space) can be built with wavelet functions. This yields a huge number of degrees of freedom and thus a very broad prior (and a difficult optimization problem when looking for the MAP point). In some applications, a level set approach ([8, 18, 31, 19]) might be more reasonable and/or efficient.

### 6.3 Hydraulic tomography

Figure 6.3 suggest that the performance of permeability inversion with wavelet priors can be improved in the setting of hydraulic tomography. This is a technique for inferring the hydraulic conductivity of a material by drilling several boreholes at different locations in the domain. Then a location is chosen as a source and hydraulic pressure is applied at that position. After equilibration of the system, pressure data is read off from all the other boreholes and the process is repeated at another well. With this technique one obtains  $N^2$  observations where  $N$  is the number of wells and the rotation of the sources typically leads to a better resolution overall.

### 6.4 Optimal experimental design

The fact that the optimization routine for obtaining the MAP point is very fast due to the nature of the wavelet transform (and the use of the adjoint method) makes it attractive in the setting of optimal experimental design. The issue is the following: Given a set of observation locations (for example in an hydraulic tomography setting) and corresponding measurements, what is the “best” location for where to take the next measurement (as rated by some information criterion like the expected uncertainty). As drilling boreholes is expensive in practice, this is a very real concern. The corresponding optimization problem can be written down in a similar way as the optimization for the MAP point. For more information about optimal experimental design, see [41] for a general overview, and a practical study [2] in the context of Bayesian inversion.

## Acknowledgments

P.W. is thankful for a fruitful discussion with Youssef Marzouk, a very helpful email from Donald Estep and in particular for the guidance of Claudia Schillings which ultimately led to the idea of this paper.

## References

- [1] S. AGAPIOU, M. BURGER, M. DASHTI, AND T. HELIN, *Sparsity-promoting and edge-preserving maximum a posteriori estimators in non-parametric bayesian inverse problems*, arXiv preprint arXiv:1705.03286, (2017).
- [2] A. ALEXANDERIAN, N. PETRA, G. STADLER, AND O. GHATTAS, *A fast and scalable method for a-optimal design of experiments for infinite-dimensional bayesian nonlinear inverse problems*, SIAM Journal on Scientific Computing, 38 (2016), pp. A243–A272.

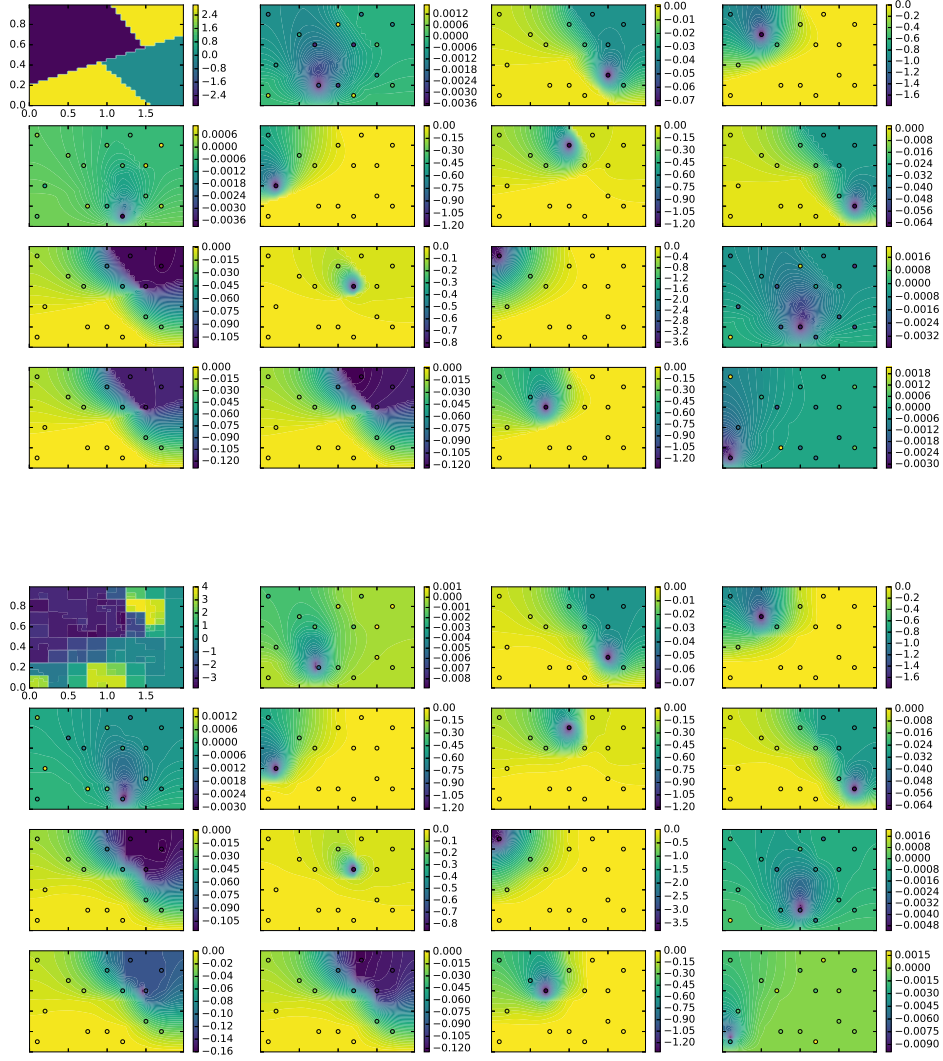


Figure 12: Reconstruction of permeability field  $e^u$  (top set of figures, top row, leftmost figure) in a 15-sources hydraulic tomography setting. The MAP reconstruction is depicted in the bottom set of figure, top row, leftmost figure. In each set of figure, the remaining 15 figures depict the pressure fields resulting from setting one observation point as a source.

- [3] M. ALNÆS, J. BLECHTA, J. HAKE, A. JOHANSSON, B. KEHLET, A. LOGG, C. RICHARDSON, J. RING, M. E. ROGNES, AND G. N. WELLS, *The fenics project version 1.5*, Archive of Numerical Software, 3 (2015), pp. 9–23.
- [4] C. BLATTER, *Wavelets: a primer*, Universities Press, 2003.
- [5] D. BLÖMKER, C. SCHILLINGS, AND P. WACKER, *A strongly convergent numerical scheme from EnKF continuum analysis*, in submission, (2017).
- [6] V. I. BOGACHEV AND V. I. BOGACHEV, *Gaussian measures*, vol. 62, American Mathematical Society Providence, 1998.
- [7] T. BUI-THANH AND O. GHATTAS, *A scalable algorithm for map estimators in bayesian inverse problems with besov priors*, Inverse Problems and Imaging, 9 (2015), pp. 27–53.
- [8] M. BURGER, *A level set method for inverse problems*, Inverse problems, 17 (2001), p. 1327.
- [9] J. CARRERA AND S. P. NEUMAN, *Estimation of aquifer parameters under transient and steady state conditions: 1. maximum likelihood method incorporating prior information*, Water Resources Research, 22 (1986), pp. 199–210.
- [10] S. CHATTERJEE AND R. DIMITRAKOPOULOS, *Multi-scale stochastic simulation with a wavelet-based approach*, Computers & geosciences, 45 (2012), pp. 177–189.
- [11] G. DA PRATO AND J. ZABCZYK, *Stochastic equations in infinite dimensions*, Cambridge university press, 2014.
- [12] M. DASHTI, S. HARRIS, AND A. STUART, *Besov priors for bayesian inverse problems*, arXiv preprint arXiv:1105.0889, (2011).
- [13] M. DASHTI AND A. M. STUART, *Uncertainty quantification and weak approximation of an elliptic inverse problem*, SIAM Journal on Numerical Analysis, 49 (2011), pp. 2524–2542.
- [14] ———, *The bayesian approach to inverse problems*, arXiv preprint arXiv:1302.6989, (2013).
- [15] I. DAUBECHIES, *Orthonormal bases of compactly supported wavelets*, Communications on pure and applied mathematics, 41 (1988), pp. 909–996.
- [16] ———, *Ten lectures on wavelets, vol. 61 of cbms-nsf regional conference series in applied mathematics*, 1992.
- [17] J. DELHOMME AND A. LAVENUE, *Four decades of inverse problems in hydrogeology*, Theory, Modeling, and Field Investigation in Hydrogeology: A Special Volume in Honor of Shlomo P. Neuman’s 60th Birthday, 348 (2000), p. 1.
- [18] O. DORN AND D. LESSELIER, *Level set methods for inverse scattering*, Inverse Problems, 22 (2006), p. R67.
- [19] M. M. DUNLOP, M. A. IGLESIAS, AND A. M. STUART, *Hierarchical bayesian level set inversion*, Statistics and Computing, (2016), pp. 1–30.

- [20] A. H. ELSHEIKH, C. PAIN, F. FANG, J. L. GOMES, AND I. M. NAVON, *Parameter estimation of subsurface flow models using iterative regularized ensemble kalman filter*, Stochastic environmental research and risk assessment, 27 (2013), pp. 877–897.
- [21] H. W. ENGL, M. HANKE, AND A. NEUBAUER, *Regularization of inverse problems*, vol. 375, Springer Science & Business Media, 1996.
- [22] D. ESTEP, *A short course on duality, adjoint operators, Green's functions, and a posteriori error analysis*, Lecture Notes, (2004).
- [23] B. G. FITZPATRICK, *Bayesian analysis in inverse problems*, Inverse problems, 7 (1991), p. 675.
- [24] J. N. FRANKLIN, *Well-posed stochastic extensions of ill-posed linear problems*, Journal of Mathematical Analysis and Applications, 31 (1970), pp. 682–716.
- [25] R. GHANEM, D. HIGDON, AND H. OWHADI, eds., *Handbook of uncertainty quantification*, Springer, 2017.
- [26] M. GILES AND P. GLASSERMAN, *Smoking adjoints: Fast monte carlo greeks*, Risk, 19 (2006), pp. 88–92.
- [27] M. B. GILES AND N. A. PIERCE, *An introduction to the adjoint approach to design*, Flow, turbulence and combustion, 65 (2000), pp. 393–415.
- [28] A. HAAR, *Zur Theorie der orthogonalen Funktionensysteme*, Mathematische Annalen, 69 (1910), pp. 331–371.
- [29] T. HELIN AND M. BURGER, *Maximum a posteriori probability estimates in infinite-dimensional bayesian inverse problems*, Inverse Problems, 31 (2015), p. 085009.
- [30] M. A. IGLESIAS, *A regularizing iterative ensemble kalman method for pde-constrained inverse problems*, Inverse Problems, 32 (2016), p. 025002.
- [31] M. A. IGLESIAS, Y. LU, AND A. M. STUART, *A bayesian level set method for geometric inverse problems*, arXiv preprint arXiv:1504.00313, (2015).
- [32] V. KOLEHMAINEN, M. LASSAS, K. NIINIMÄKI, AND S. SILTANEN, *Sparsity-promoting bayesian inversion*, Inverse Problems, 28 (2012), p. 025005.
- [33] H.-H. KUO, *Gaussian measures in banach spaces*, in Gaussian Measures in Banach Spaces, Springer, 1975, pp. 1–109.
- [34] M. LASSAS, E. SAKSMAN, AND S. SILTANEN, *Discretization-invariant bayesian inversion and besov space priors*, Inverse Problems and Imaging, 3 (2009), pp. 87–122.
- [35] A. LOGG, K.-A. MARDAL, AND G. WELLS, *Automated solution of differential equations by the finite element method: The FEniCS book*, vol. 84, Springer Science & Business Media, 2012.
- [36] S. G. MALLAT, *Multiresolution approximations and wavelet orthonormal bases of  $L^2(\mathbb{R})$* , Transactions of the American mathematical society, 315 (1989), pp. 69–87.
- [37] A. MANDELBAUM, *Linear estimators and measurable linear transformations on a hilbert space*, Zeitschrift für Wahrscheinlichkeitstheorie und Verwandte Gebiete, 65 (1984), pp. 385–397.

- [38] Y. MEYER, *Wavelets and operators*, vol. 1, Cambridge university press, 1995.
- [39] A. NEUBAUER AND H. K. PIKKARAINEN, *Convergence results for the bayesian inversion theory*, Journal of Inverse and Ill-posed Problems, 16 (2008), pp. 601–613.
- [40] M. PANZERI, M. RIVA, A. GUADAGNINI, AND S. P. NEUMAN, *Comparison of ensemble kalman filter groundwater-data assimilation methods based on stochastic moment equations and monte carlo simulation*, Advances in Water Resources, 66 (2014), pp. 8–18.
- [41] F. PUKELSHEIM, *Optimal design of experiments*, SIAM, 2006.
- [42] M. RANTALA, S. VANSKA, S. JARVENPAA, M. KALKE, M. LASSAS, J. MOBERG, AND S. SILTANEN, *Wavelet-based reconstruction for limited-angle x-ray tomography*, IEEE transactions on medical imaging, 25 (2006), pp. 210–217.
- [43] A. RIEDER, *A wavelet multilevel method for ill-posed problems stabilized by tikhonov regularization*, Numerische Mathematik, 75 (1997), pp. 501–522.
- [44] C. SCHILLINGS AND A. M. STUART, *Analysis of the ensemble kalman filter for inverse problems*, arXiv preprint arXiv:1602.02020, (2016).
- [45] A. M. STUART, *Inverse problems: a bayesian perspective*, Acta Numerica, 19 (2010), pp. 451–559.
- [46] T. J. SULLIVAN, *Introduction to uncertainty quantification*, vol. 63, Springer, 2015.
- [47] N.-Z. SUN, *Inverse problems in groundwater modeling*, vol. 6, Springer Science & Business Media, 2013.
- [48] N.-Z. SUN AND W. W.-G. YEH, *Identification of parameter structure in groundwater inverse problem*, Water Resources Research, 21 (1985), pp. 869–883.
- [49] H. TRIEBEL, *Function spaces and wavelets on domains*, vol. 7, European Mathematical Society, 2008.
- [50] Z. WANG, J. M. BARDSLEY, A. SOLONEN, T. CUI, AND Y. M. MARZOUK, *Bayesian inverse problems with  $l_1$  priors: a randomize-then-optimize approach*, arXiv preprint arXiv:1607.01904, (2016).